Experimental Verification of Numerical Model for Nonlinear Wave Evolutions

By Takumi Ohyama,[1] Serdar Beji,[2] Kazuo Nadaoka,[3] and Jurjen A. Battjes[4]

INTRODUCTION

It is known that relatively long waves passing over a submerged bar decompose into shorter components. The power spectra measured in front of and behind such barred topographical regions differ appreciably because the latter spectrum contains significant energy over a broad range in the high-frequency band (Ohyama and Nadaoka 1992; Beji and Battjes 1993). These waveform evolutions result from shoaling over the upslope and near-resonant wave-wave interactions over the bar, which transfers energy to higher harmonics. Under such circumstances nonlinear effects may significantly affect the wave evolution.

Longuet-Higgins and Cokelet (1976) successfully applied the boundary integral equation method (BIEM) to the computation of evolving nonlinear surface waves. Numerous alternative models have been presented since (Vinje and Brevig 1981; Dold and Peregrine 1984; Grilli et al. 1989). It has been confirmed that transient wave evolutions for a short period of time are well predicted by these models, even in the case of plunging breakers (Dommermuth et al. 1988). However, especially for spectral transformation of random waves, quantitative comparisons between predictions and observations have rarely been provided.

The purpose of this study is to furnish such comparisons for the demanding case of deformation and decomposition of near-breaking waves passing over a submerged bar. The model tested here was developed by Ohyama and Nadaoka (1991).

EXPERIMENTS

The wave flume and the submerged bar used in the experiments are sketched in Fig. 1. A piston-type random-wave generator was installed at an end of the flume, and a plane beach with coarse material was placed as a wave absorber at the other end. The reflection coefficient of this beach was of the order of 5% (Van Leeuwen 1992). The free-surface displacements were measured with parallel-wire resistance gauges at seven different locations (Fig. 1). The time history of the wave-paddle displacement was also recorded. The sampling frequency was 25.4 Hz.

[1]Res. Sci., Envir. Engrg. Dept., Inst. of Tech., Shimizu Corp., Etchujima 3-4-17, Koto-ku, Tokyo 135, Japan.

[2]Post-doctorate Fellow, Dept. of Oc. Engrg., Istanbul Tech. Univ., Maslak 80626, Istanbul, Turkey.

[3]Assoc. Prof., Dept. of Civ. Engrg., Tokyo Inst. of Technol., Ō-okayama, Meguro-ku, Tokyo 152, Japan.

[4]Prof., Dept. of Civ. Engrg., Delft Univ. of Technol., P.O. Box 5048, 2600 GA Delft, The Netherlands.

Note. Discussion open until May 1, 1995. To extend the closing date one month, a written request must be filed with the ASCE Manager of Journals. The manuscript for this technical note was submitted for review and possible publication on February 3, 1993. This technical note is part of the ***Journal of Waterway, Port, Coastal, and Ocean Engineering***, Vol. 120, No. 6, November/December, 1994. ©ASCE, ISSN 0733-950X/94/0006-0637/$2.00 + $.25 per page. Technical Note No. 5568.

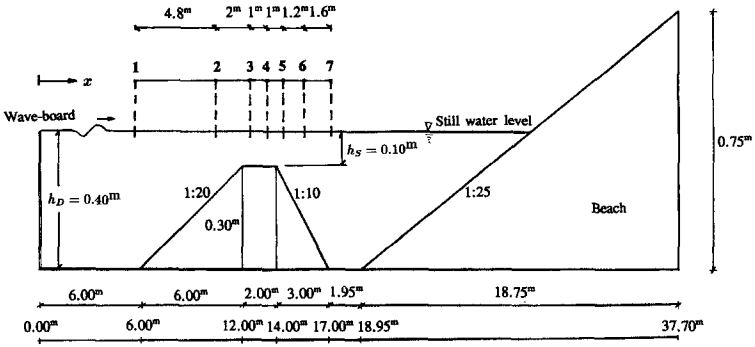

FIG. 1. Wave Flume and Locations of Wave Gages

TABLE 1. Mesh Size Used in Computations

Incident waves (1)	Frequency ($f_0\sqrt{h_D/g}$; $f_p\sqrt{h_D/g}$) (2)	Mesh size on free surface ($\Delta x/L$) (3)
Monochromatic waves	0.1010	1/15 ($0 \le x/h_D \le 19$) 1/40 ($x/h_D \ge 19$)
	0.1616	1/15 ($0 \le x/h_D \le 25$) 1/30 ($x/h_D \ge 25$)
Random waves	0.1010	1/20 ($0 \le x/h_D \le 19$) 1/40 ($x/h_D \ge 19$)
	0.1616	1/20 ($0 \le x/h_D \le 25$) 1/30 ($x/h_D \ge 25$)

Four different measurements were obtained: two different spectral shapes (monochromatic waves with a spike spectrum and random waves with a JONSWAP target spectrum), with two different peak frequencies (0.5 Hz and 0.8 Hz, referred to as the "long" waves and the "short" waves, respectively). All the measurements reported here were the nonbreaking waves. However, it was important that the incident wave heights were large enough to develop into finite-amplitude waves over the bar crest so that associated waveform transformations could be observed. The following incident wave heights H_0 to the water depth h_D ratios were selected for the monochromatic waves: $H_0/h_D = 0.05$ and 0.0625 for the long and short waves, respectively. The random waves required somewhat smaller incident significant wave heights $H_{1/3}$ to prevent occasional breaking, and we used $H_{1/3}/h_D = 0.045$ and 0.0575 for the long and short waves, respectively. The initial wave heights of the high-frequency cases were larger than their low-frequency counterparts because it was attempted to keep the nonlinearity parameter, ε = amplitude/water-depth, nearly the same in the shallowest region.

NUMERICAL MODEL

Computations were carried out with a numerical model, previously developed by Ohyama and Nadaoka (1991). The model, solving the equations for the irrotational flow of an inviscid liquid, is based on the BIEM with nonreflective open boundaries. In the present calculations, we utilized the

same wave-generating method as was used in the model experiments, namely that

$$\frac{\partial \phi}{\partial x} = U(t) \quad \text{(on the left side boundary)} \tag{1}$$

where ϕ = velocity potential and U = horizontal velocity of the wave paddle. At the right end of the domain, a numerical wave-absorption filter was placed for the open boundary treatment, corresponding to the wave-absorber used in the experiments.

Mesh size on the free surface used in the computations is indicated in Table 1, in which L is the incident wave length (corresponding to the peak frequency for random waves), and f_0 and f_p are the peak frequencies of monochromatic and random incident waves, respectively. In all the computations, the time increment Δt was set to 1/32 of the incident wave period (spectral peak period for random waves). For the random waves, $\Delta x/L$ in the initial propagation domain was smaller than that for the monochromatic waves to capture the higher-frequency components. The surface of the submerged bar was discretized into 110 fixed elements in all cases, resulting in $\Delta x/L$ = 1/38 and 1/20 for the long and short waves, respectively.

The inputs to the numerical model were the bottom profile, the still-water level, and the time history of the wave-board displacement. The initial condition was zero surface displacement and velocity throughout the computational domain.

The subsequent discussion utilizes numerical results after 10 periods for the long waves and after 20 periods for the short waves from the cold start.

COMPARISONS OF MEASUREMENTS AND COMPUTATIONS

Fig. 2 show the comparisons of the measured and computed wave profiles for the case of the long monochromatic waves, where η is the surface elevation. The overall agreement is excellent, especially in the upslope region and over the horizontal portion. In the downslope, some minor dif-

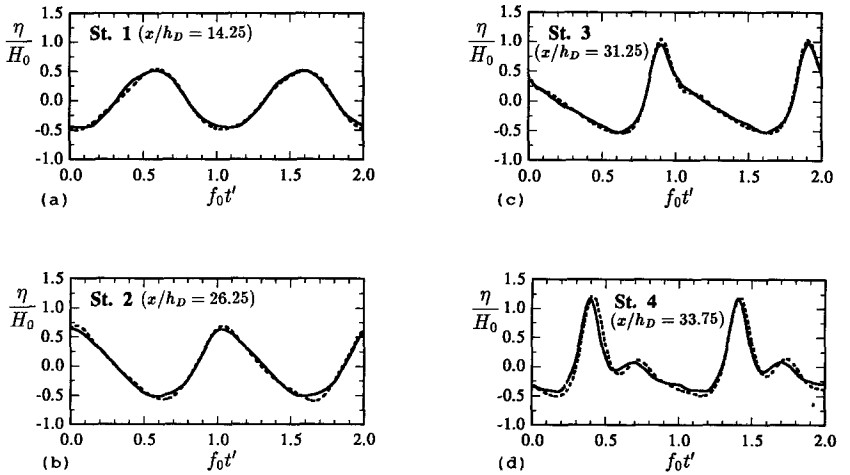

FIG. 2. Measured (——) and Computed (- - - -) Wave Profiles for Long Monochromatic Waves ($f_0\sqrt{h_D/g}$ = 0.1010) at Stations 1–7

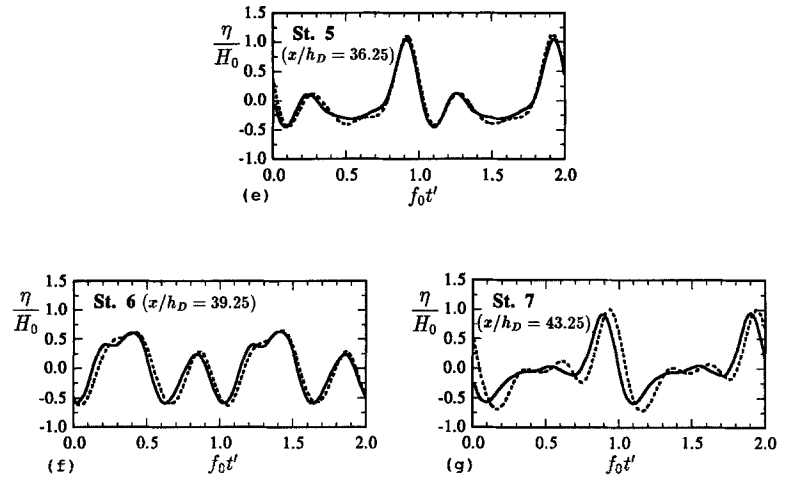

FIG. 2. (*Continued*)

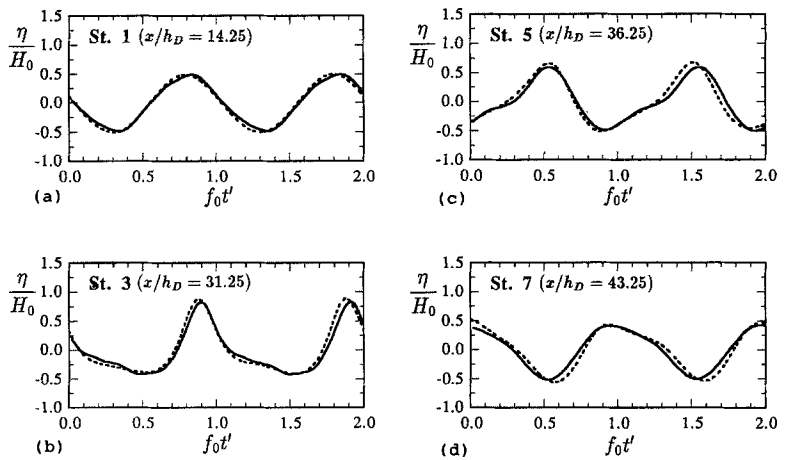

FIG. 3. Measured (——) and Computed (- - - -) Wave Profiles for Short Monochromatic Waves ($f_0\sqrt{h_D/g}$ = 0.1616) at Stations 1, 3, 5, and 7

ferences are observed between the measurements and computations. These discrepancies may be attributed to insufficient spatial resolution in the downslope because, in this region, waves with smaller wavelengths become dominant. Consequently, the initially adopted resolution could become relatively coarse.

It is worthwhile to observe how the initially sinusoidal wave form evolves as it travels over the bar. At station 2 the wave has a saw-toothed shape with the slight forward pitch that is characteristic for waves on a plane beach. The waveform at station 4 in the shallowest region is clearly reminiscent of the soliton formation behind a solitary wave propagating into a shallower depth. Due to the harmonic decomposition, the waveforms in the deepening section (stations 5–7) are substantially different from each other and those from previous stations.

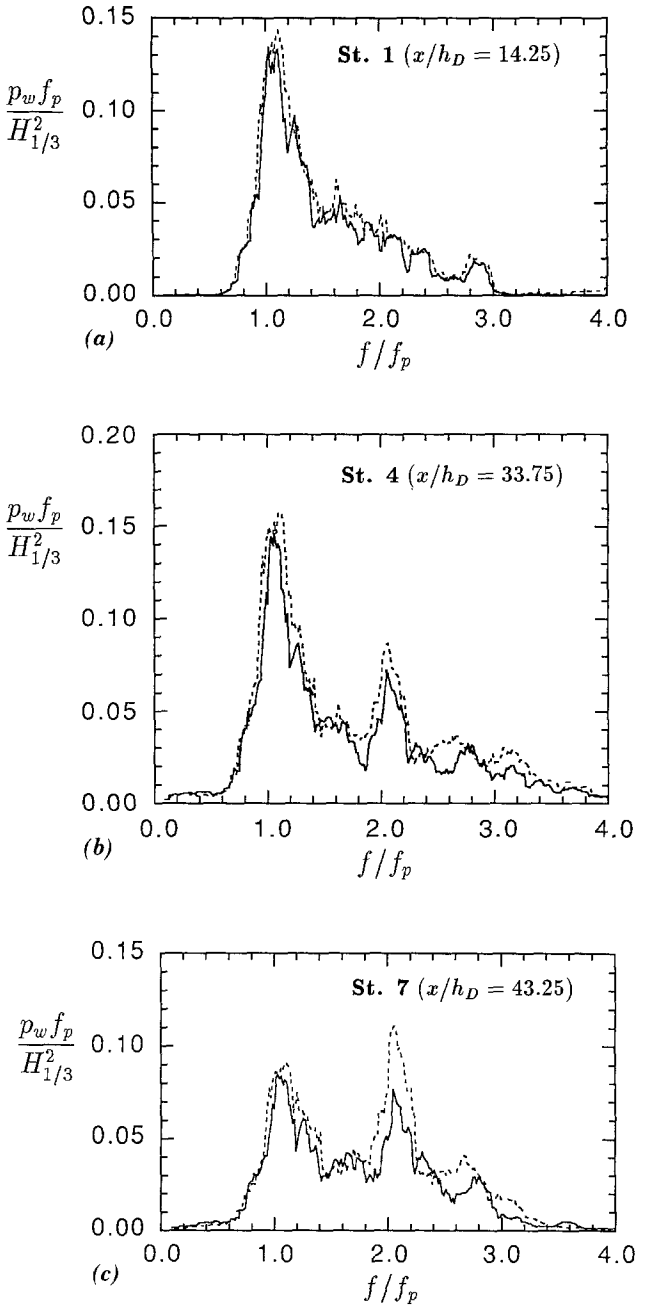

FIG. 4. Measured (——) and Computed (- - - -) Power Spectra of Long Random Waves ($f_p\sqrt{h_D/g} = 0.1010$) at Stations 1, 4, and 7

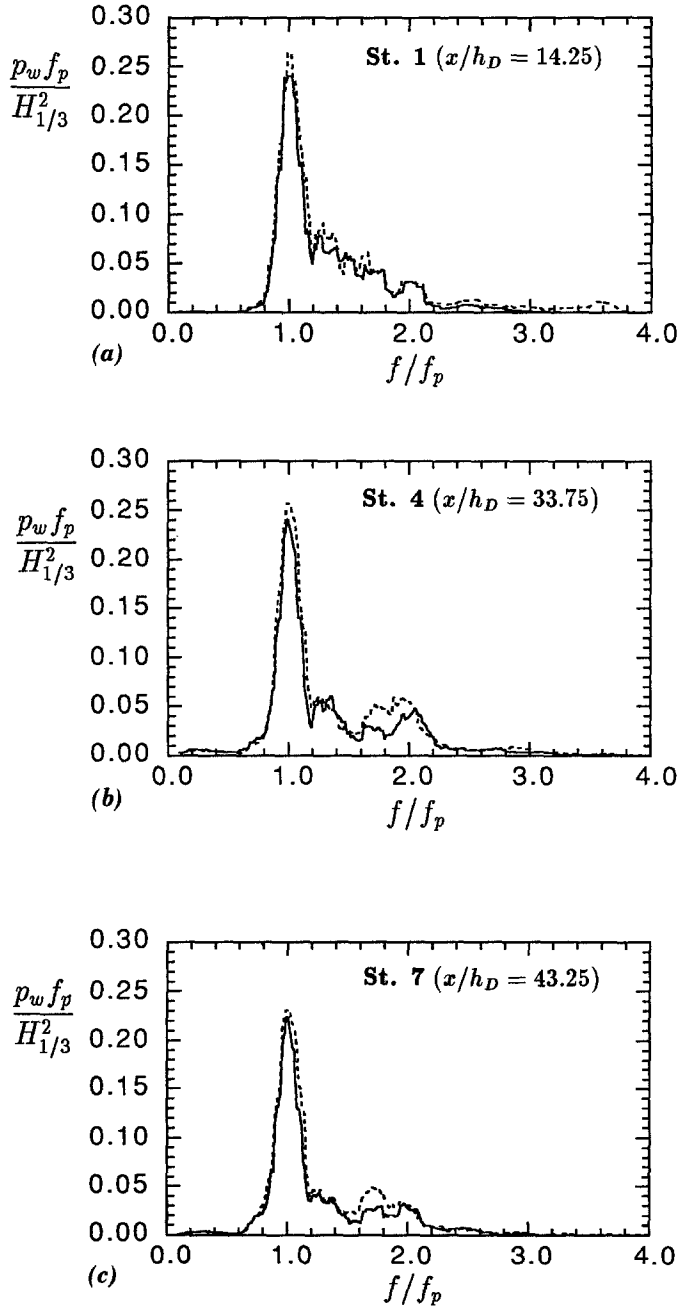

FIG. 5. Measured (——) and Computed (- - - -) Power Spectra of Short Random Waves ($f_p\sqrt{h_D/g} = 0.1616$) at Stations 1, 4, and 7

Fig. 3 shows the results for the short monochromatic wave (only for stations 1, 3, 5, and 7). The waveform appears like a higher order Stokes-type deepwater wave and it does not evolve appreciably. In this case, the difference in wave number between free and bound wave components in the higher harmonics is markedly larger than that for the long-wave case, indicating that the near-resonant conditions are not satisfied. Consequently, the growth rate of the higher harmonics remains low and the waveforms in the deeper regions are not much different from those at the first two stations. The agreement for the waveforms in this case is quite favorable. Minor discrepancies in the wave amplitude may be due to the fact that the dissipation effect is not taken into account in the numerical model.

For the random incident waves, comparisons are given only for the power spectra p_w at stations 1, 4, and 7 (Figs. 4 and 5). These power spectra were obtained from the time records for a duration of $63/f_p$. The sliding-average technique was applied to the raw spectra obtained from the measured and computed surface profiles. For each group of 11 neighboring raw spectral values, the sixth value in the group was replaced by the average of those 11 values.

For the longer waves, the spectral evolution is substantial, and so is the amount of high-frequency energy generation during these nonlinear evolutions (Fig. 4). The corresponding numerical results overestimate the higher harmonics at station 7 but agree reasonably well for the measured primary components. In contrast, a negligible amount of high-frequency energy generation is observed for the shorter waves (Fig. 5). In this case the discrepancy between the measured and computed spectra is quite small.

The numerical model effectively predicts the overall evolution of the energy spectra, but some differences in amplitudes and phases were found in the time-domain records, even in the constant-depth section between wave generator and slope. These discrepancies are attributed to numerical errors in the phase speed of incident higher-frequency components. Although a finer mesh would improve accuracy, it does not, at present, justify the corresponding increase in central processing unit (CPU) cost.

CONCLUSIONS

Overall, the agreement between the measurements and the computations is satisfactory. For the monochromatic "long" and "short" waves, the numerical model performs well, with excellent agreement between the measured and computed waveforms. Although some minor discrepancies are observed for the random waves, the performance of the model remains acceptable, indicating its reliability for the prediction of a nonlinear random-wave transformation.

The absence of dissipation in the computational model results in some discrepancies in the wave energy. However, that may not be a serious shortcoming for applications, since the dissipation is relatively smaller at prototype scales. As computing costs continue to decrease, numerical models such as the one presented here will find wider use in engineering applications.

APPENDIX. REFERENCES

Beji, S., and Battjes, J. A. (1993). "Experimental investigation of wave propagation over a bar." *Coast. Engrg.*, Vol. 19, 151–162.

Dold, J. W., and Peregrine, D. H. (1984). "Steep unsteady waves: an efficient

computational scheme." *Proc., 19th Int. Conf. Coast. Engrg.*, ASCE, New York, N.Y. 955–967.
Dommermuth, D. G., Yue, D. K. P., Lin, W. M., Rapp, R. J., Chan, E. S., and Melville, W. K. (1988). "Deep-water plunging breakers: a comparison between potential theory and experiments." *J. Fluid Mech.*, Vol. 189, 423–442.
Grilli, S. T., Skourup, J., and Svendsen, I. A. (1989). "An efficient boundary element method for nonlinear water waves." *Engrg. Anal. with Boundary Element*, Vol. 6, 97–107.
Longuet-Higgins, M. S., and Cokelet, E. D. (1976). "The deformation of steep surface waves on water. 1. a numerical method of computation." *Proc., Royal Soc.*, London, England, A 350, 1–26.
Mei, C. C. (1989). *The applied dynamics of ocean surface waves*. World Scientific Publishing, Singapore, 578–593.
Ohyama, T., and Nadaoka, K. (1991). "Development of a numerical wave tank for analysis of nonlinear and irregular wave field." *Fluid Dynamics Res.*, Vol. 8, 231–251.
Ohyama, T., and Nadaoka, K. (1992). "Modeling the transformation of nonlinear wave train passing over a submerged dike." *Proc., 23rd Int. Conf. Coast. Engrg.*, ASCE, New York, N.Y. 526–539.
Van Leeuwen, P. J. (1992). "Low frequency wave generation due to breaking waves," PhD thesis, Delft University of Technology, Delft, The Netherlands.
Vinje, T., and Brevig, P. (1981). "Numerical simulation of breaking waves." *Adv. Water Resour.*, Vol. 4, 77–82.